Research Square

Preprints are preliminary reports that have not undergone peer review.
They should not be considered conclusive, used to inform clinical practice,
or referenced by the media as validated information.

SIRT5-mediated desuccinylation prevents mitochondrial dysfunction in Alveolar epithelial cells senescence and Pulmonary fibrosis

Wenyu Hou
University of Electronic Science and Technology of China
Yunmulan Zhao
University of Electronic Science and Technology of China
Fei Li
Second Hospital of Tianjin Medical University
Zexin Guo
Second Hospital of Tianjin Medical University
Liqing Yang
Sichuan Academy of Medical Sciences & Sichuan Provincial People's Hospital
Chunyan Duan
Sichuan Academy of Medical Sciences & Sichuan Provincial People's Hospital
Lingyun Gao
Sichuan Academy of Medical Sciences & Sichuan Provincial People's Hospital
Wei Sun
dlswdoc@163.com

Second Hospital of Tianjin Medical University

Research Article

Keywords: Idiopathic pulmonary fibrosis, Alveolar epithelial cells, Aging, Mitochondrial dysfunction, SIRT5, Lysine succinylation

Posted Date: July 15th, 2024

DOI: https://doi.org/10.21203/rs.3.rs-4594800/v1

License: This work is licensed under a Creative Commons Attribution 4.0 International License.
Read Full License

Additional Declarations:

No competing interests reported.

Supplementary Material S2-S5 are not available with this version

SIRT5-mediated desuccinylation prevents mitochondrial dysfunction in Alveolar epithelial cells senescence and Pulmonary fibrosis

Wenyu Hou[3], Yunmulan Zhao[3], Lingyun Gao[2], Fei Li[1], Zexin Guo[1], Liqing Yang[2,3], Chunyan Duan[2,3], Wei Sun[1]

1, Department of Respiratory and Critical Care Medicine, The Second Affiliated Hospital of Tianjin Medical University, Tianjin, 300211, China

2, Department of Respiratory and Critical Care Medicine, Sichuan Provincial People's Hospital, Chengdu, 610072, China

3, University of Electronic Science and Technology of China, Chengdu, 611731, China

Wenjue Hou, Yunmulan Zhao, and Lingyun Gao share the first author.

Corresponding authors: Wei Sun is the corresponding author. E-mail address: dlswdoc@163.com.

Abstract

Background Senescence of alveolar epithelial cells (AEC) is a key event in the occurrence and development of Idiopathic pulmonary fibrosis (IPF). The pathogenic mechanisms that underlie the effects of AEC senescence remain largely unexplained. Some age-related diseases have an etiology that is related to mitochondrial dysfunction induced by excessive lysine succinylation (Ksucc). Excessive Ksucc levels can be removed by SIRT5 to maintain mitochondrial homeostasis.

Aims The aim of this study was to determine the effects of SIRT5-mediated de-Ksucc on mitochondrial function and pulmonary fibrosis after AEC senescence

Methods The expressions of Ksucc and SIRT5 were observed by western blot and immunofluorescence. The mitochondrial morphology of aging AEC was observed by Transmission electron microscopy (TEM). The effect of SIRT5-mediated desuccinylation on mitochondrial function and aging fibrotic effect was determined by using SA-β-gal, mitoSOX, and MitoTracker staining. liquid chromatography with tandem mass spectrometry (LC-MS/MS) to perform the first global profiling of Ksucc in lung tissues with IPF patients. The changes of candidate key proteins and Ksucc sites

related to energy metabolism in IPF lung tissues were analyzed by using the clusters of orthologous groups of proteins (COG), Kyoto Encyclopedia of Genes and Genomes (KEGG) and Gene ontology (GO). Specific succinylated proteins were validated by parallel reaction monitoring (PRM).

Results AEC in the lungs of IPF patients exhibit a marked accumulation of dysmorphic and dysfunctional mitochondria and excessive Ksucc levels. These mitochondrial abnormalities in AEC of normal mice with advancing age were associated with the downregulation of SIRT5. Increase SIRT5 expression in aging AEC maintains mitochondrial function and reduces fibrotic effects of AEC senescence in established bleomycin (BLM)-aging mouse model. 1964 Ksucc sites in 628 proteins were identified and specific succinylated proteins (GRHPR, HSD17B8) were closely related to mitochondria functions in the IPF lungs. SIRT5 down-regulate the Ksucc level of GRHPR and HSD17B8 in the AEC aging model.

Conclusions HyperKsucc is the basis of mitochondrial dysfunction in the AEC senescence and SIRT5 alleviates the pulmonary fibrosis induced by AEC senescence by stabilizing the mitochondrial function.

Keywords Idiopathic pulmonary fibrosis. Alveolar epithelial cells. Aging. Mitochondrial dysfunction. SIRT5. Lysine succinylation

Abbreviations

IPF Idiopathic pulmonary fibrosis

AEC Alveolar epithelial cells

PTM Post-translational modification

Ksucc Lysine succinylation

PGCα1 Peroxisome proliferator-activated receptor-C gamma coactivator-1α

mtDNA/gDNA Mitochondrial to genomic DNA

TFAM Transcription factor A mitochondrial

COG Clusters of orthologous groups of proteins

PRM Parallel reaction monitoring

GO Gene ontology

KEGG The Kyoto Encyclopedia of Genes and Genomes

TEM Transmission electron microscopy

Introduction

The latest epidemiological study found that the median age of diagnosis of Idiopathic pulmonary fibrosis (IPF) is approximately 65 years, which indicates that IPF is an age-related disease (Hambly et al. 2022). The mechanisms involved in aging-related IPF susceptibility are still unknown. One of the most accepted theories and our previous studies showed in the pathogenesis of IPF is that alveolar epithelial cells (AEC) showed obvious characteristics of aging characteristics leading to the secretion of profibrotic cytokines and fibroblast activation (Cui et al. 2022; Jing et al. 2022).

Mitochondria are particularly susceptible to age (Nguyen et al., 2023). Abnormalities in mitochondria are often observed with aging cells, including mitochondrial DNA damage, oxidative stress, energy metabolism disorders, and cell apoptosis (Vue et al. 2023; Han et al. 2023). Mitochondrial is regulated by a variety of post-translational modifications of proteins (LeFort et al. 2024). Lysine succinylation (Ksucc) is thought to have an important role in the maintenance of mitochondrial morphology and function and the selective degradation of damaged mitochondria. Ksucc is a naturally occurring post-translational modification (PTM) that regulates the stability and function of proteins and is different from acetylation as the succinyl group is bulkier and causes a greater change in charge than an acetyl group (Zhao et al. 2023; Shen et al. 2023). However, AEC in the lung are active progenitors and secretory cells containing approximately 50% of lung mitochondrial mass (Hong et al. 2023; Lee et al. 2023), so it is reasonable to speculate that AEC senescence in IPF may be due to the occurrence of mitochondrial hyperKsucc.

SIRT5, a mitochondrial sirtuin with very weak deacetylase activity, is a potent desuccinylase, the catalytic reaction involves the removal of a succinyl group from the lysine side chain of protein substrates (Wei et al. 2024). SIRT5 as a global regulator of Ksucc in mitochondria has been reported that sirtuins depletion is related to the progression of pulmonary fibrosis, and increasing expression of sirtuins protein plays a protective role in pulmonary fibrosis (Shaikh et al. 2019). Although the precise role of

SIRT5 in pulmonary fibrosis has not yet been reported, recent studies have confirmed that SIRT5 prevents cell senescence by maintaining mitochondrial function, regulating mitochondrial metabolism, and inhibiting oxidative stress response (Hong et al. 2024). Therefore, we speculated that SIRT5-mediated deKsucc could prevent the AEC senescence and the occurrence of pulmonary fibrosis by stabilizing mitochondrial function.

Our present studies showed that aging lungs have an hperKsucc and dysfunctional mitochondria in aging AEC, a key process that triggers SIRT5 upregulation to maintain the stability of mitochondrial function and reduce activation of profibrotic responses induced by AEC senescence.

Materials and method

Collection of human lung tissue

This study was approved by the Ethics Committee of The Second Affiliated Hospital of Tianjin Medical University and Sichuan Provincial People's Hospital. IPF lung tissue samples ($n = 6$) and Paracancerous control lung tissues ($n = 6$) were obtained from the Department of Lung Transplantation, Sichuan Provincial People's Hospital, Cheng Du, China. Diagnostic criteria for IPF refer to the guidance of the 2022 ATS/ERS/JRS/ALAT guideline (Raghu et al. 2022).

Animals and animal treatment

Male C57BL/6 mice at 8 weeks of age and aged mice (12 and 24-month-old mice) were obtained from the Animal Center, Tianjin Medical University (Tianjin, China) and housed in a standard environment with a regular light/dark cycle and free access to water and chow diet.

All treatment procedures for mice were based on endotracheal injection after anesthesia and described amply by others. The lentivirus-packaged pcDNA (1×10^8 TU/mL, 100 μL/mouse) was administered 1 day before bleomycin (BLM)

（BioDuly, A0109） injection in 12-week-old male mice. After 21 days post bleomycin injection, the mice were killed, and lungs were collected for subsequent experiments.

Isolation of AEC cells and fibroblasts culture

Mouse AEC was obtained from 12-month-old mice (2 mice per isolation) as previously reported (Yang et al. 2022; Sun et al. 2021). Briefly, human AEC isolated from fresh peripheral lung tissue obtained from IPF lung tissue samples and Paracancerous control lung tissues were digested with a mixture of dispase (Sigma-Aldrich), collagenase (Sigma-Aldrich), and DNAseI (Sigma-Aldrich), using a Gentle MACS (Miltenyi) dissociation instrument using negative selection. The supernatants containing non-adherent, human AEC were collected, pooled, and centrifuged at 300×g for 10 min. The resulting pellet was resuspended in 100 mL isolation medium without DNase and plated again on new plastic culture dishes, followed by incubation for 45 min. This second panning step was performed at least 2 times. Finally, these supernatants containing enriched, non-adherent human AEC were collected pooled, and centrifuged at 300×g for 10 min. Human AEC were identified using optical microscopy. According to this technique, more than 95% of the cells were AEC.

Human embryonic lung fibroblast MRC5 cells were purchased from the American Type Culture Collection (Priscilla, CL-0161). The cells were cultured in DMEM/F12 with 1% penicillin/streptomycin and 10% FBS at 37 ℃ under 5% CO2.

Histopathology, immunofluorescence, and transmission electron microscopy

After sacrifice, lungs were perfused with 2% paraformaldehyde (sharp, BL539A), followed by paraformaldehyde embedding or saturation in 30% sucrose for 24 hours for frozen sections. Paraffin sections were stained with H&E or Masson trichrome (Solarbio, G1340) to determine changes in fibrosis.

Human lung tissue sections were deparaffined with xylene for 20 min twice and rehydrated in gradient-reduced ethanol (100% twice, 95%, 90%, 75%, and 50% once) for 5 min each. Antigen retrieval was performed for 30 min at 95 ℃ using 0.01 M sodium citrate buffer (Solarbio, C1010). The sections were then blocked for 1 h with 5% FBS in PBST at room temperature. For human lung tissue, the slides were incubated with primary antibodies as follows: rabbit anti-surfactant protein C (SP-C) antibody (Abcam, ab90716), mouse anti-P16 antibody (SANTA, sc-1661), rabbit anti-SIRT5 antibody (SANTA, sc-271635), mouse anti-PGCα1 (Abcam, ab191838). For mouse lung tissue, immunofluorescence staining is the same as for human lung tissue. The secondary antibodies were Alexa Fluor 488-conjugated goat anti-rabbit IgG antibody (proteintech, SA00013-2) and Alexa Fluor 594-conjugated goat anti-mouse IgG antibody (proteintech, SA00013-3), incubated for 1 h at room temperature.

For transmission electron microscopy (TEM), lung tissue was fixed in 3% glutaraldehyde and 2% paraformaldehyde in 0.1 M sodium cacodylate buffer at pH 7.3. Morphometric analyses (number of mitochondria per cell and mitochondrial size) were performed using NIH ImageJ (version 1.43). At least 10 cells from low-magnification images (×10,000) were used to count the number of mitochondria per AEC (identified by the presence of lamellar bodies). At least 100–150 individual mitochondria, from 3 different lungs per group at high magnification (×25,000 and ×50,000), were used to assess perimeter and area.

LV-SIRT5pcDNA interference and real-time PCR

Lentivirus-packaged pcDNA was purchased from GenePharma *Co. Ltd* for in vitro and in vivo experiments. All transfection procedures were carried out according to the instructions. Primary mice AEC were seeded in a 6-well plate and replenished with a medium containing 1 × 107 TU/mL lentivirus and 5 μg/mL polybrene. After incubating for 24 h, replenish AEC with fresh DMEM/F12 complete medium and continue culture for 48 h. The intervention efficiency was tested in primary AEC in vivo and in vitro by qPCR.

Total RNA isolation was carried out using the TRIzol RNA isolation system (Life Technologies) according to the manufacturer's instructions. The first strand of complementary DNA was synthesized using 1 μg of RNA in 20 μl of reaction buffer containing AMV-RT (Life Technologies) and random primers at 42°C for 60 min. Real-time PCR was performed using a Platinum SYBR Green qPCR SuperMix-UDG (Invitrogen, 11733046). The resultant cDNA was used as the template for the quantitative real-time PCR step using a LightCycler instrument (Roche, Mannheim, Germany) according to the manufacturer's manual. The relative quantification of target gene expression was performed using glyceraldehyde-3-phosphate dehydrogenase (GAPDH) mRNA as the internal control. The targeted genes were amplified using the following primers:

5′-GCCATAGCCGAGTGTGAGAC-3′ (forward) and 5′-CAACTCCACAAGAGGTACATCG-3′ (reverse) for SIRT5 (Human);

5′-GCCACCGACAGATTCAGGTT-3′ (forward) and 5′-CCACAGGGCGGTTAAGAAGT-3′ (reverse) for SIRT5 (Mouse);

Western blot analysis

The lung tissue or cultured cells were homogenized in lysis buffer and their protein concentrations were measured using a Bradford assay. Protein samples were separated by 10% SDS-PAGE and transferred to a polyvinylidene fluoride (PVDF) membrane (Millipore, IPVH00010). The samples were incubated with primary antibodies overnight at 4 ℃. The membranes were incubated with horseradish peroxidase (HRP)-conjugated secondary antibody at room temperature for 1 h, and the immunoreactive protein bands were detected using a chemiluminescence device (GE, Amersham imager 680). The levels of protein expression were evaluated by measuring the gray value of the band by Fiji software, $n = 3$ in each group, and the relative value to β-actin was compared. The primary antibodies used were as follows: anti-p16 (SANTA, sc-1661), anti-PGCα1 (Abcam, ab191838), anti-SIRT5 (SANTA, sc-271635), anti-α-SMA (Abcam, ab240654), and anti-CollagenI (Abcam, ab260043).

Immunoprecipitation

AEC from different groups was collected, washed twice with ice-cold PBS, dissolved in cold radioimmunoprecipitation assay (RIPA) lysis buffer, and then incubated on ice for 30 min. After centrifugation at 12,000 × g for 15 min at 4 °C, Cell lysates (500 μg) were then incubated with 2 μg of anti-HSD17B8 (Abcam, ab169752) or anti-GRHPR (Abcam, ab155604) antibody for 2 h at 4 °C on a rocker platform (30 rocks/min). Protein-antibody complexes were collected with 20 μl of Protein G PLUS Agarose (Santa Cruz Biotechnology, CA, USA) on a rocker platform (30 rocks/min) overnight at 4 °C. Te immunoprecipitates were washed three times with lysis buffer. Equal amounts (10 μg/lane) of proteins were subjected to 12% SDS-PAGE for succinylation antibodies (1:50; Jingjie Biology, Hangzhou, China) at 4 °C.

MitoSOX, MitoTracker staining, and SA-β-gal

Cultured cells were stained for ROS production via mitoSOX and mitochondria via MitoTracker deep red according to the manufacturer's instructions. Frozen sections (3 μm) were used for the detection of mitochondria via MitoTracker deep red (Beyotime, C1049B) staining according to the manufacturer's instructions. The Senescence β-Galactosidase Staining Kit was purchased from Cell Signaling Technology (Solarbio, G1580). Cell samples on 6-well dishes were fixed with 4% formaldehyde for 10 min at room temperature. The cells were washed three times with PBS for 5 min and then incubated with freshly prepared SA-β-Gal staining solution overnight a 37° C. The next day, the stained cells were imaged under a Zeiss Axio Observer inverted microscope using differential interference contrast brightfield microscopy (DIC). For each slide, at least three fields were captured to calculate the SA-β-gal intensity.

mtDNA/gDNA ratio

DNA was purified from the primary AEC, generated with the TRI-reagent/Chloroform RNA extraction, according to the manufacturer's protocol (Sigma-Aldrich, Zwijndrecht, the Netherlands), with the modification of centrifugation speed to 12,000 g. DNA was pelleted, and dissolved in TE buffer (Merck, 93283). qPCR was performed as described previously with mitochondrial (COX-II) and genomic (RPL13A) specific primers.
5′-ATGCTCGCCCGCGCCCTGCTGCTGT-3′ (forward) and 5′-ACAGCAGCAGGGCGCGGGCGAGCAT-3′ (reverse) for COX-II (Human);
5′-TGCACTATGGTTACAAAAGCTGG-3′ (forward) and 5′-TCAGGAAGCTCCTTATTTCCCTT-3′ (reverse) for COX-II (Mouse);
5′-GCCCTACGACAAGAAAAAGCG-3′ (forward) and 5′-TACTTCCAGCCAACCTCGTGA-3′ (reverse) for RPL13A (Human);
5′-AGCCTACCAGAAAGTTTGCTTAC-3′ (forward) and 5′-GCTTCTTCTTCCGATAGTGCATC-3′ (reverse) for RPL13A (Mouse);
Data is presented as a ratio of the relative copy number of mtDNA over gDNA.

LC-MS/MS analysis

The tryptic peptides were dissolved in solvent A (0.1% FA, 2% ACN in water), and directly loaded onto a homemade reversed-phase analytical column (25 cm length, 100 μm i.d.). Peptides were separated with a gradient from 6% to 22% solvent B (0.1% FA in ACN) over 40 min, 22% to 30% in 12 min, and climbing to 80% in 4 min then holding at 80% for the last 4 min, all at a constant flow rate of 450 nL/min on a nanoElute UHPLC system (Bruker Daltonics).

The peptides were subjected to a Capillary source followed by the times of Pro (Bruker Daltonics) mass spectrometry. The electrospray voltage applied was 1.60 kV. Precursors and fragments were analyzed at the TOF detector, with an MS/MS scan range from 100 to 1700 m/z. The timsTOF Pro was operated in parallel accumulation serial fragmentation (PASEF) mode. Precursors with charge states 0 to 5 were selected for fragmentation, and 10 PASEF-MS/MS scans were acquired per cycle. The dynamic exclusion was set to 24s.

Gene ontology annotation and Kyoto Encyclopedia of Genes and Genomes pathway annotation

Gene ontology (GO) is a major bioinformatics initiative to unify the representation of genes and gene product attributes across all species. The GO annotation proteome was derived from the UniProt-GOA database (www. http://www.ebi.ac.uk/GOA/). First, the identified protein ID was converted to UniProt ID and was then mapped to GO IDs using the protein ID. If the identified proteins were not annotated by the UniProt-GOA database, the InterProScan software was used to annotate the protein's GO function based on a protein sequence alignment method. Then, the proteins were classified by GO annotation into three categories: biological process, cellular component, and molecular function.

The Kyoto Encyclopedia of Genes and Genomes (KEGG) database was used to annotate the protein pathways. First, the KEGG online service tool KAAS was used to annotate the protein's KEGG database description. Then, the annotation result was mapped on the KEGG pathway database using the KEGG online service tool KEGG Mapper.

Parallel reaction monitoring annotation (PRM)

IPF lung tissue samples (n=3) and Paracancerous lung tissue samples (n=3) were verified by the PRM validation experiment. The PRM-MS assay was performed on Q Exactive HF-X MS spectrometer and peptides were separated with the following gradient: 0-36 min, 9%-25%B, 36-54 min, 25%-35%B, 54-57 min, 35%-80%B, 57-60 min, 80%B, and all at a constant flow rate of 500 nl/minon a EASY-nLC 1200 UPLC system (ThermoFisher Scientific). The digested peptides for differential proteins and endogenous peptides identified from DDA-MS analysis with appropriate sequence length and MS/MS spectrum were programmed for the PRM assay. The full mass scan range was set as 495 - 1234 with a resolution of 120000. The MS/MS scans were

acquired by the Orbitrap with a resolution of 15000. The collisional energy was 28%, and the AGC target was set to 1e5 with a maximum injection time of 220 ms for MS/MS.

Statistical analyses

All data examined were expressed as mean ± SEM. Statistical significance between the two groups was estimated using the unpaired two-tailed Student's t-test. One-way ANOVA and post hoc Tukey's test were performed for comparing more than two groups. $p < 0.05$ was considered significant. All statistical analyses were performed using GraphPad Prism 9.0.

Results

Aging AEC from IPF lungs show an accumulation of dysfunctional mitochondria and hperKsucc

In this study, we collected lung tissues from IPF patients to observe whether Ksucc has occurred in IPF lung tissue. Firstly, HE and Masson staining were used to determine the pathological status of lung tissue of IPF and paracancerous control lung tissues (Fig. 1A). Furtherly, the results of pan-succinylation antibody detection result showed that the total protein in lung tissue of IPF patients was modified from 12KDa to 130KDa through Western blot (Fig. 1B). We also detected expression of SIRT5 which is desuccinylation key enzyme, reflecting levels of deKsucc in mitochondria in the IPF lung. Western blotting results showed that compared with the control group, SIRT5 protein expression was down-regulated in IPF lungs (Fig. 1C). This indicated that aging lungs are closely related to the hyKsucc of mitochondria.

We hypothesized that changes in mitochondrial homeostasis in the AEC from the lungs of IPF patients might compromise AEC senescence. We examined mitochondria in aged AEC by immunofluorescence analyses in lung sections of IPF patients using SP-C and peroxisome proliferator-activated receptor-C gamma coactivator-1α (PGCα1)

which are mitochondrial biogenesis-related transcription factors, as markers of AEC and mitochondria, respectively. As shown in the result, the expressions of PGC-1α and P16 (Aging marker) were significantly up-regulated in aging AEC from IPF patients. However, SIRT5 as key enzymes for deKsucc and key proteins for mitochondrial function protection confirmed the lower protein expression levels in aged AEC (Fig. 2A). Because AEC forms the cell compartment that contains the majority of the lung mitochondrial mass (Ma et al. 2023), we therefore isolated mitochondria from control lungs and IPF lungs. The changes in mitochondria in aging AEC were further confirmed by electron microscopy. Morphometric analyses of electron microscopy images demonstrated that mitochondria in IPF lung AEC were enlarged and dysmorphic, with significantly increased mitochondrial area and number of mitochondria per cell contrast to contrast to AEC from Lung tissue adjacent to cancer (Fig. 2B-E). Mitochondrial content was also estimated by the ratio of mitochondrial to genomic DNA (mtDNA/gDNA). The mtDNA/ gDNA ratio was significantly increased in AEC in IPF patient lungs, but not AEC from Lung tissue adjacent to cancer (Fig. 2F). The above results suggest that mitochondrial dysfunction occurs in aged AEC and is associated with decreased SIRT5 expression in IPF.

The expression of SIRT5 is age-dependent in dysfunctional mitochondria of aging AEC

We need to study the changes in mitochondrial function and SIRT5 in old adult C57BL/6 mice (7, 12, 24 months). Pathological staining was performed on mice of different ages, and the results showed that the number of cells in lung interstitial and the blue-dyed collagen fibers increased with the increase of age, and the 24 months mice were the most obvious (Fig. 3A). Immunofluorescence showed that PGC-1α and P16 gradually upregulated with age, while SIRT5 gradually downregulated, especially by 24 months of age (Fig. 3B-C).

Primary AEC was isolated from old adult C57BL/6 mice (7, 12, 24 months). We investigated the mitochondrial biogenesis-related transcription factors PGC-1α and transcription factor A, mitochondrial (TFAM), two master regulators governing

mitochondrial biogenesis. As shown in Western blotting results, PGC-1α and TFAM were upregulated with age, but SIRT5 was down-regulated, especially by 24 months of age (Fig. 4A). AEC senescence was analyzed by β-galactosidase (SA-β-gal) activity, the result showed the number of senescent AEC of 12 months of age increased compared with that of 7 months of age, and the AEC of 24 months of age were the most obvious (Fig. 4B)

We analyzed AEC mitochondrial function by MitoTracker deep red staining and mitochondrial ROS by mitoSOX staining. Mitochondrial content was significantly increased in the AEC of 12-month-old mice, and the 24-month-old mice were the most obvious (Fig. 4C-D). The mitoSOX staining showed that mitochondrial ROS production increased in aging AEC progressively over the time points assessed (Fig. 4E). Mitochondrial content was also estimated by the ratio of mitochondrial to genomic DNA (gDNA). The mtDNA/ gDNA ratio was significantly increased in AEC from 24 months of age (Fig. 4F). Together, these data suggest that despite the accumulation of dysfunctional mitochondria in ACE from aging lungs.

SIRT5 ameliorates age-related impairment of dysfunctional mitochondria in BLM-aging model

To further examine whether SIRT5-mediated deKsucc regulates mitochondrial dysfunction in age-related lung fibrosis, lentivirus-packaged LV-*SIRT5*pcDNA was constructed. we pretreated BLM-induced old mice (12 months) with a single intratracheal LV-*SIRT5*pcDNA in vivo and LV-*SIRT5*pcDNA interferes with the BLM-induced aging model of AEC in vitro (Supplementary 1). Immunofluorescence analyses in vivo revealed that compared with the expression of normal adults (12 months of age), PGC-1α increased in AEC of lung tissues by BLM-induced mice, and significantly downregulated in mice injected with LV-*SIRT5*pcDNA. Compared with the BLM-treated mice, the expression of SIRT5 in AEC of lung tissues significantly increased in LV-*SIRT5*pcDNA-treated old mice. (Fig. 5A-B). We further analyzed lung mitochondrial mass by MitoTracker deep red staining, mitochondrial mass was

significantly increased in 12-month-old mice and less in mice injected with LV-*SIRT5*pcDNA (Fig. 5C-D).

To further verify the experimental results in vivo, Western blot analyses and immunofluorescence in vitro revealed AEC from old mice (12 months) treated with BLM 72h, PGC-1α, and TFAM significantly increased, however LV-*SIRT5*pcDNA significantly reversed these proteins expression. (Fig. 6A-B). We further analyzed AEC mitochondrial mass in 12-month-old mice by MitoTracker deep red staining, mitochondrial ROS by mitoSOX staining, and the ultrastructural analysis of mitochondria using electron microscopy. Mitochondrial mass, and mitochondrial ROS production were significantly increased, and mitochondria were enlarged, mitochondrial area and number of mitochondria per cell also were significantly increased in AEC treated with BLM 72h. However, LV-*SIRT5*pcDNA ameliorates these pathological phenomena (Fig. 6C-D). The mtDNA/ gDNA ratio was significantly increased in AEC treated with BLM, and desuccinylation by LV-*SIRT5*pcDNA declined mtDNA content in AEC from 12- 12-month-old mice (Fig. 6E).

The removal of Ksucc by LV-SIRT5pcDNA inhibits AEC senescence in an established BLM-aging model

We examined the effects of SIRT5-mediated deKsucc on AEC senescence in BLM-treated AEC. In vivo, BLM was injected through mouse bronchus and treated with LV-*SIRT5*pcDNA. As shown in the result, compared with the control group (12 months of age), P16, the key marker of aging, was most significantly up-regulated in AEC marked by SPC of BLM-induced old mice. LV-*SIRT5*pcDNA significantly downregulated P16 expression in the AEC of BLM-induced mice (Fig. 7A). HE and Masson's trichrome staining showed that Bronchial drip of *LV-SIRT5*pcDNA improved the pathology of BLM-induced pulmonary fibrosis in 12-month-old mice (Fig. 7B).

In vitro, β-galactosidase staining showed that after LV-*SIRT5*pcDNA treatment, the number of AEC induced by BLM decreased significantly (Fig. 7C). AEC was transfected with LV-*SIRT5*pcDNA and exposed to BLM to induce aging, the expression

of P16 was also significantly down-regulated by using Western blot, and immunofluorescence. (Fig. 7D-E). The supernatants of senescent AEC were collected to culture the fibroblast cell line MRC-5 for 3 days. We found that the levels of α-SMA and collagen I, which are hallmarks of myofibroblasts, were both higher in MRC-5 cells cultured in senescent conditioned medium (SASP-CM) compared with those in cells cultured control conditioned medium (CCM). The levels of α-SMA and collagen I were downregulated significantly via LV-*SIRT5*pcDNA in the SASP-CM group (Fig. 7F).

Global profiling of lysine succinylation in lung tissues with IPF patients

The aforementioned experimental results have confirmed that hyperKsucc leads to AEC senescence by participating in mitochondrial dysfunction, so we performed a proteomic study of Ksucc in IPF lung tissues. Altogether, 1964 succinylation sites on 628 proteins were identified after the database search (Supplementary 2). To identify potential specific sequence patterns associated with Ksucc sites, we utilized the MoMo analysis tool. The analysis revealed a thermogram displaying the score of amino acid frequency changes near the Ksucc site (Fig. 8A). Within the regions surrounding succinylated peptides, three enriched conserved motifs were identified. Valine (V), aspartic acid (D), and alanine (A) residues were found to be the most common in succinylated sequences, with 173, 144, and 145 succinylated peptides, respectively (Fig. 8B).

To better understand the function of succinylated proteins in IPF lung tissues, a subcellular localization analysis was performed by using UniProt database notes. The majority of the succinylated proteins were localized in mitochondria (44.75%), the rest of the succinylated proteins were located in the cytoplasm (25.96%), extracellular (13.38%), nucleus (7.17%), plasma membrane (3.18%), endoplasmic reticulum (2.23%), cytoplasm, nucleus (2.07%) and other (1.27%) (Fig. 8C). To further elucidate the potential role of succinylated proteins in IPF, we analyzed the data for GO enrichment and KEGG PATHWAY analysis. In the KEGG PATHWAY analysis, the results showed that these succinylated proteins were enriched in pathways associated with mitochondrial metabolism, including amino acid degradation, TCA cycle, and

fatty acid degradation (Fig. 8D) (Supplementary 3). In the GO enrichment analysis, the majority of succinylated proteins showed significant enrichment in CC (Cellular Components) related to mitochondria (Fig. 8E) (Supplementary 4).

SIRT5 is required for mitochondrial energy metabolism in AEC

In mitochondrial metabolism, glucose metabolism and lipid metabolism are the most closely related to the progression of pulmonary fibrosis (Chung et al. 2019; Zhang et al. 2023). According to the screening results of the succinylation proteomics and KEGG analysis, GRHPR and HSD17B8 were validated by PRM. GRHPR were enriched in the KEGG Pyruvate metabolism (hsa00620) and Glycine, serine, and threonine metabolism (hsa00260) pathway and HSD17B8 were enriched in Fatty acid biosynthesis (hsa00061) (Supplementary 3). The PRM validation results revealed notable differences in expression between the IPF groups and the control groups. Compared with the control groups, the sites in GRHPR and HSD17B8 exhibited upregulation, reaching statistical significance ($P < 0.05$) (Fig. 9A) (Supplementary 5).

Furthermore, we intervened in the aging model of AEC in vitro using *SIRT5*pcDNA and used the immunoprecipitation technique to investigate whether SIRT5 can regulate GRHPR and HSD17B8. The immunoprecipitation in vitro showed that the BLM group significantly upregulated GRHPR and HSD17B8 protein expression and also increased GRHPR and HSD17B8 succinylation levels compared with the control group. However, compared with the BLM group, the succinylation levels of GRHPR and HSD17B8 were decreased in response to *SIRT5*pcDNA, and the GRHPR and HSD17B8 protein expression did not decrease (Fig. 9B).

Discussion

Aging is a risk factor for many chronic disorders, including IPF (Wang et al. 2023). The available evidence suggests that a common denominator for age-related diseases is a decline in mitochondrial function (Hofer et al. 2021). Here, we showed that hyperKsucc

is the basis of age-related mitochondrial dysfunction in the AEC senescence in the pathogenesis of IPF. We confirmed SIRT5-mediated deKsucc alleviated the accumulation of dysfunctional mitochondria in the senescent AEC of IPF lungs.

Similar to our present findings, studies in the lung suggest that mitochondrion is the major organelle that supplies energy and maintains cellular homeostasis to keep essential organ functions (Starinets et al. 2022; Huang et al. 2023). Notably, the accumulation of damaged mitochondria probably plays a key role in triggering cellular senescence and accelerating aging (Victorelli et al. 2023). Hence, a better understanding of mitochondrial dysfunction would be of great significance to ameliorate aging.

Ksucc is the dynamic changes of post-translational modification of mitochondrial proteins relating to age-related mitochondrial dysfunction (Kubatzky et al. 2023). HyperKsucc occurs in mitochondria, which destroy mitochondrial homeostasis and trigger cellular senescence (Lancaster et al. 2023). Conversely, removing hyperKsucc in mitochondria can slow aging by protecting mitochondria (Park et al. 2013). Ksucc, acetylation, and malonylation are all directly regulated by the Sirtuin protein family, and SIRT5 in the Sirtuin protein family is a very important deKsucc by sensing cellular REDOX status and energy metabolism requirements (Guo et al. 2018; Teng et al. 2024; Tong et al. 2021). We observed that mitochondrial content, mitochondrial ROS production, and energy-synthesizing substances were increased in AEC of BLM-old mice lungs and human IPF lungs. Mitochondrial materials such as mtDNA that leak from damaged mitochondria have been reported to elucidate inflammatory responses (Zhou et al. 2021). Our present data also support mtDNA levels elevated in AEC senescence for reflecting a potential role of dysfunctional mitochondria in pulmonary fibrosis. Consistent with the foregoing notion, we also found that the total protein of senescent AEC is generally modified by Ksucc, while SIRT5 expression is down-regulated. It is noteworthy that in an established age-associated pulmonary fibrosis model induced by BLM, the administration of *SIRT5*pcDNA, removing the hyperKsucc, reduces cellular AEC senescence, and retard pulmonary fibrosis by protecting mitochondrial functions. These data demonstrate the potent therapeutic effects on age-

related pulmonary fibrosis by promoting SIRT5 expression even after mitochondrial dysfunction and AEC senescence have occurred.

Similar to our present findings, the Ksucc is involved in many core energy metabolism pathways and affects the metabolic process in mitochondria, making this modification highly valuable for studying diseases related to mitochondrial disorder (Hou et al. 2024; Zeng et al. 2020). To further clarify the detailed mechanism of the effect of succinylation on mitochondrial dysfunction in pulmonary fibrosis and whether SIRT5 can also be the target of this potential mechanism, we applied Ksucc proteomics technology to analyze the lung tissue proteins and their modification sites in IPF patients. Here, we found that the 628 identified succinylated proteins have 1964 SuK sites, and 44.75% protein is located in mitochondria. These proteins located in the mitochondria are mainly related to mitochondrial metabolism, including amino acid degradation, TCA cycle, and fatty acid degradation. At present, in cellular energy metabolism, glycolysis and lipid metabolism are most closely related to the progression of pulmonary fibrosis (Xu et al. 2021; Tong et al. 2024). After risk assessment of the screened proteins around these two metabolites, we decided to validate HSD17B8 and GRHPR by PRM and immunoprecipitation. We found that there were significant differences in the Ksucc sites of GRHPR and HSD17B8 between the lung tissues of IPF patients and the normal lung tissues, and the expression levels of these proteins were increased in the AEC senescence induced by BLM. However, the Ksucc was removed by increasing the expression of SIRT5, the succinylation levels of these proteins were down-regulated. These results suggest that SIRT5-mediated desuccinylation affects mitochondrial function mainly through metabolic pathways in AEC senescence.

Conclusion

Our present findings indicated that hyperKsucc is critically involved in age-related mitochondrial dysfunction and pulmonary fibrotic lesions. SIRT5-mediated deKsucc could provide better AEC senescence blockade and protect mitochondrial functions, thereby slowing age-related pulmonary fibrosis. These data provide proof of the

principle that targeted induction of SIRT5 protects against aging by preventing mitochondrial dysfunction in the treatment of fibrotic lung diseases.

Acknowledgements The authors thank Lingyun Gao and Liqing Yang from the Department of Respiratory and Critical Care Medicine, Sichuan Provincial People's Hospital, Chengdu, China for their generous gifts of IPF lung tissue samples. We also thank PTM Biolabs (Hangzhou, China) for support of Ksucc proteomic analysis.

Author contributions Wenyu Hou, Yunmulan Zhao, and Lingyun Gao performed the research and wrote this paper; Wei Sun designed the study; Fei Li and Zexin Guo analyzed the data; Chunyan Duan and Liqing Yang provided clinical samples; Lingyun Gao and Wei Sun provided fund support. All authors read and approved the final manuscript.

Funding This work was supported by the Sichuan Natural Science Foundation (No. 23NSFSC1556) and, the Key R&D Plan of the Sichuan Provincial Department of Science and Technology (No. 23ZDYF1850).

Data availability The datasets and materials generated and/or analyzed during the current study are available from the corresponding author on reasonable request

Declarations

Ethics approval and consent to participate

Animal experiments were approved by the Ethics Committee of Tianjin Medical University. The experiments were conducted in consideration of the ARRIVE guidelines

Consent for publication Not applicable.

Competing interests The authors declare no competing interest

References

Chung KP, Hsu CL, Fan LC, Huang ZL, Bhatia D, Chen YJ, Hisata S, Cho SJ, Nakahira K, Imamura M, Choi ME, Yu CJ, Cloonan SM, Choi AMK. Mitofusins regulate lipid metabolism to mediate the development of lung fibrosis. Nature Communications. 2019;10. https://doi.org/10.1038/s41467-019-11327-1

Guo D, Song XH, Guo TF, Gu SG, Chang XL, Su T, Yang XH, Liang B, Huang DY. Vimentin acetylation is involved in SIRT5-mediated hepatocellular carcinoma migration. American Journal of Cancer Research. 2018;8:2453-66.

Hambly N, Farooqi MM, Dvorkin-Gheva A, Donohoe K, Garlick K, Scallan C, Chong SG, MacIsaac S, Assayag D, Johannson KA, Fell CD, Marcoux V, Manganas H, Morisset J, Comes A, Fisher JH, Shapera S, Gershon AS, To T, Wong AW, Sadatsafavi M, Wilcox PG, Halayko AJ, Khalil N, Cox G, Richeldi L, Ryerson CJ, Kolb M. Prevalence and characteristics of progressive fibrosing interstitial lung disease in a prospective registry. European Respiratory Journal. 2022;60. https://doi.org/10.1183/13993003.02571-2021

Han SHY, Lee MH, Shin Y, Giovanni R, Chakrabarty RP, Herrerias MM, Dada LA, Flozak AS, Reyfman PA, Khuder B, Reczek CR, Gao L, Lopez-Barneo J, Gottardi CJ, Budinger GRS, Chandel NS. Mitochondrial integrated stress response controls lung epithelial cell fate. Nature. 2023;620. https://doi.org/10.1038/s41586-023-06423-8

Hofer SJ, Liang YT, Zimmermann A, Schroeder S, Dengjel J, Kroemer G, Eisenberg T, Sigrist SJ, Madeo F. Spermidine-induced hypusination preserves mitochondrial and cognitive function during aging. Autophagy. 2021;17:2037-9. https://doi.org/10.1080/15548627.2021.1933299

Hong JR, Jin L, Zhang CY, Zhong WJ, Yang HH, Wang GM, Ma SC, Guan CX, Li Q, Zhou Y. Mitochondrial citrate accumulation triggers senescence of alveolar epithelial cells contributing to pulmonary fibrosis in mice. Heliyon. 2023;9. https://doi.org/10.1016/j.heliyon.2023.e17361

Hong JY, Raza SHA, Ma HM, Cao WN, Chong YQ, Wu J, Xi DM, Deng WD. Multiple omics analysis reveals the regulation of SIRT5 on mitochondrial function and lipid metabolism during the differentiation of bovine preadipocytes. Genomics. 2024;116. https://doi.org/10.1016/j.ygeno.2023.110773

Hou XL, Chen YQ, Li X, Gu XL, Dong WX, Shi J, Ji SP. Protein succinylation: regulating metabolism and beyond. Frontiers in Nutrition. 2024;11. https://doi.org/10.3389/fnut.2024.1336057

Huang T, Lin RY, Su YQ, Sun H, Zheng XX, Zhang JS, Lu XY, Zhao BQ, Jiang XC, Huang LL, Li N, Shi J, Fan XH, Xu DH, Zhang TY, Gao JQ. Efficient intervention for pulmonary fibrosis via mitochondrial transfer promoted by mitochondrial biogenesis. Nature Communications. 2023;14. https://doi.org/10.1038/s41467-023-41529-7

Jing XY, Sun W, Yang XY, Huang H, Wang P, Luo Q, Xia S, Fang CL, Zhang Q, Guo J, Xu ZJ. CCAAT/enhancer-binding protein (C/EBP) homologous protein promotes alveolar epithelial cell senescence via the nuclear factor-kappa B pathway in pulmonary fibrosis. International Journal of Biochemistry

& Cell Biology. 2022;143. https://doi.org/10.1016/j.biocel.2021.106142

Kubatzky KF, Gao Y, Yu D. Post-translational modulation of cell signalling through protein succinylation. Exploration of targeted anti-tumor therapy. 2023;4:1260-85. https://doi.org/10.37349/etat.2023.00196

Lancaster MS, Kim B, Doud EH, Tate MD, Sharify AD, Gao HY, Chen DJ, Simpson E, Gillespie P, Chu XA, Miller MJ, Wang Y, Liu YL, Mosley AL, Kim J, Graham BH. Loss of succinyl-CoA synthetase in mouse forebrain results in hypersuccinylation with perturbed neuronal transcription and metabolism. Cell Reports. 2023;42. https://doi.org/10.1016/j.celrep.2023.113241

Lee KY, Yang CC, Shueng PW, Wu SM, Chen CH, Chao YC, Chang YC, Han CL, Chuang HC, Lee CC, Lin CW. Downregulation of TAZ elicits a mitochondrial redox imbalance and ferroptosis in lung epithelial cells exposed to diesel exhaust particles. Ecotoxicology and Environmental Safety. 2023;266. https://doi.org/10.1016/j.ecoenv.2023.115555

LeFort KR, Rungratanawanich W, Song BJ. Contributing roles of mitochondrial dysfunction and hepatocyte apoptosis in liver diseases through oxidative stress, post-translational modifications, inflammation, and intestinal barrier dysfunction. Cellular and Molecular Life Sciences. 2024;81. https://doi.org/10.1007/s00018-023-05061-7

Liu G, Cui H, Xie N, Banerjee S, Liu R, Antony VB, Sanders YY, Thannickal VJ, Kaminski N. CD38 Mediates Lung Fibrosis by Promoting Alveolar Epithelial Cell Aging. American Journal of Respiratory and Critical Care Medicine. 2022;205.

Ma M, Gao YJ, Qiu XH, Gui XH, Tian YQ, Tian M, Albertson TE, Kishaba T, Tanino Y, Sakairi Y, Chen JY, Dai JH, Cai HR. ZLN005 improves the protective effect of mitochondrial function on alveolar epithelial cell aging by upregulating PGC-1α. Journal of Thoracic Disease. 2023;15:6160-77. https://doi.org/10.21037/jtd-23-815

Nguyen TT, Wei S, Nguyen TH, Jo Y, Zhang Y, Park W, Gariani K, Oh C-M, Kim HH, Ha K-T, Park KS, Park R, Lee I-K, Shong M, Houtkooper RH, Ryu D. Mitochondria-associated programmed cell death as a therapeutic target for age-related disease. Experimental & Molecular Medicine. 2023;55:1595-619. https://doi.org/10.1038/s12276-023-01046-5

Park J, Chen Y, Tishkoff DX, Peng C, Tan MJ, Dai LZ, Xie ZY, Zhang Y, Zwaans BMM, Skinner ME, Lombard DB, Zhao YM. SIRT5-Mediated Lysine Desuccinylation Impacts Diverse Metabolic Pathways. Molecular Cell. 2013;50:919-30. https://doi.org/10.1016/j.molcel.2013.06.001

Raghu G, Remy-Jardin M, Richeldi L, Thomson CC, Inoue Y, Johkoh T, Kreuter M, Lynch DA, Maher TM, Martinez FJ, Molina-Molina M, Myers JL, Nicholson AG, Ryerson CJ, Strek ME, Troy LK, Wijsenbeek M, Mammen MJ, Hossain

T, Bissell BD, Herman DD, Hon SM, Kheir F, Khor YH, Macrea M, Antoniou KM, Bouros D, Buendia-Roldan I, Caro F, Crestani B, Ho L, Morisset J, Olson AL, Podolanczuk A, Poletti V, Selman M, Ewing T, Jones S, Knight SL, Ghazipura M, Wilson KC, Amer Thoracic S, European Resp S, Japanese Resp S, Assoc Latinoamer T. Idiopathic Pulmonary Fibrosis (an Update) and Progressive Pulmonary Fibrosis in Adults An Official ATS/ERS/JRS/ALAT Clinical Practice Guideline. American Journal of Respiratory and Critical Care Medicine. 2022;205:E18-E47. https://doi.org/10.1164/rccm.202202-0399ST

Shaikh SB, Prabhu A, Bhandary YP. Targeting anti-aging protein sirtuin (Sirt) in the diagnosis of idiopathic pulmonary fibrosis. Journal of Cellular Biochemistry. 2019;120:6878-85. https://doi.org/10.1002/jcb.28033

Shen R, Ruan HY, Lin SY, Liu B, Song H, Li L, Ma T. Lysine succinylation, the metabolic bridge between cancer and immunity. Genes & Diseases. 2023;10:2470-8. https://doi.org/10.1016/j.gendis.2022.10.028

Starinets VS, Serov DA, Penkov NV, Belosludtseva NV, Dubinin MV, Belosludtsev KN. Alisporivir Normalizes Mitochondrial Function of Primary Mouse Lung Endothelial Cells Under Conditions of Hyperglycemia. Biochemistry-Moscow. 2022;87:605-16. https://doi.org/10.1134/s0006297922070033

Sun W, Jing XY, Yang XY, Huang H, Luo Q, Xia S, Wang P, Wang N, Zhang Q, Guo J, Xu ZJ. Regulation of the IGF1 signaling pathway is involved in idiopathic pulmonary fibrosis induced by alveolar epithelial cell senescence and core fucosylation. Aging-Us. 2021;13:18852-69.

Teng P, Cui KS, Yao SR, Fei BJ, Ling F, Li CQ, Huang ZH. SIRT5-mediated ME2 desuccinylation promotes cancer growth by enhancing mitochondrial respiration. Cell Death and Differentiation. 2024;31:65-77. https://doi.org/10.1038/s41418-023-01240-y

Tong YY, Guo D, Lin SH, Liang JZ, Yang DQ, Ma CM, Shao F, Li M, Yu QJ, Jiang YH, Li L, Fang J, Yu RL, Lu ZM. SUCLA2-coupled regulation of GLS succinylation and activity counteracts oxidative stress in tumor cells. Molecular Cell. 2021;81:2303-+. https://doi.org/10.1016/j.molcel.2021.04.002

Tong ZK, Du XK, Zhou Y, Jing FX, Ma JP, Feng YY, Lou SY, Wang Q, Dong ZX. Drp1-mediated mitochondrial fission promotes pulmonary fibrosis progression through the regulation of lipid metabolic reprogramming by ROS/HIF-1α. Cellular Signalling. 2024;117. https://doi.org/10.1016/j.cellsig.2024.111075

Victorelli S, Salmonowicz H, Chapman J, Martini H, Vizioli MG, Riley JS, Cloix C, Hall-Younger E, Espindola-Netto JM, Jurk D, Lagnado AB, Gomez LS, Farr JN, Saul D, Reed R, Kelly G, Eppard M, Greaves LC, Dou ZX, Pirius N, Szczepanowska K, Porritt RA, Huang HJ, Huang TY, Mann DA, Masuda CA, Khosla S, Dai HM, Kaufmann SH, Zacharioudakis E, Gavathiotis E, Lebrasseur NK, Lei X, Sainz AG, Korolchuk VI, Adams PD, Shadel GS, Tait

SWG, Passos JF. Apoptotic stress causes mtDNA release during senescence and drives the SASP (vol 622, pg 627, 2023). Nature. 2024;625:E15-E. https://doi.org/10.1038/s41586-023-07002-7

Vue Z, Garza-Lopez E, Neikirk K, Katti P, Vang L, Beasley H, Shao JQ, Marshall AG, Crabtree A, Murphy AC, Jenkins BC, Prasad P, Evans C, Taylor B, Mungai M, Killion M, Stephens D, Christensen TA, Lam J, Rodriguez B, Phillips MA, Daneshgar N, Koh HJ, Koh A, Davis J, Devine N, Muhammod S, Scudese E, Arnold KR, Chavarin VV, Robinson RD, Chakraborty M, Gaddy JA, Sweetwyne MT, Wilson G, Zaganjor E, Kezos J, Dondi C, Reddy AK, Glancy B, Kirabo A, Quintana AM, Dai DF, Ocorr K, Murray SA, Damo SM, Exil V, Riggs B, Mobley BC, Gomez JA, McReynolds MR, Hinton A. 3D reconstruction of murine mitochondria reveals changes in structure during aging linked to the MICOS complex. Aging Cell. 2023;22. https://doi.org/10.1111/acel.14009

Wang L, Zhu MH, Li Y, Yan PS, Li ZZ, Chen XP, Yang JT, Pan X, Zhao HB, Wang SH, Yuan HM, Zhao MX, Sun XG, Wan RY, Li F, Wang XB, Yu HT, Rosas I, Ding C, Yu GY. Serum Proteomics Identifies Biomarkers Associated With the Pathogenesis of Idiopathic Pulmonary Fibrosis. Molecular & Cellular Proteomics. 2023;22. https://doi.org/10.1016/j.mcpro.2023.100524

Wei C, Shi MX, Dong SY, Li ZT, Zhao BB, Liu D, Li GP, Cen J, Yu LG, Liang X, Shi LL. SIRT5-related lysine demalonylation of GSTP1 contributes to cardiomyocyte pyroptosis suppression in diabetic cardiomyopathy. International Journal of Biological Sciences. 2024;20:585-605. https://doi.org/10.7150/ijbs.83306

Xu Q, Cheng DM, Li GR, Liu Y, Li P, Sun WQ, Ma DY, Ni CH. CircHIPK3 regulates pulmonary fibrosis by facilitating glycolysis in miR-30a-3p/FOXK2-dependent manner. International Journal of Biological Sciences. 2021;17:2294-307. https://doi.org/10.7150/ijbs.57915

Yang XY, Sun W, Jing XY, Zhang Q, Huang H, Xu ZJ. C/EBP homologous protein promotes Sonic Hedgehog secretion from type II alveolar epithelial cells and activates Hedgehog signaling pathway of fibroblast in pulmonary fibrosis. Respiratory Research. 2022;23. https://doi.org/10.1186/s12931-022-02012-x

Zeng FY, Pang HY, Chen Y, Zheng HW, Li WX, Ramanathan S, Hoare R, Monaghan SJ, Lin XM, Jian JC. First Succinylome Profiling of Vibrio alginolyticus Reveals Key Role of Lysine Succinylation in Cellular Metabolism and Virulence. Frontiers in Cellular and Infection Microbiology. 2021;10. https://doi.org/10.3389/fcimb.2020.626574

Zhang JM, Chen WM, Du JZ, Chu LH, Zhou ZL, Zhong WS, Liu DY, Huang HH, Huang Y, Qiao YJ, Meng XJ, Zou F, Cai SX, Dong HM. RNF130 protects against pulmonary fibrosis through suppressing aerobic glycolysis by mediating c-myc ubiquitination. International Immunopharmacology.

2023;117. https://doi.org/10.1016/j.intimp.2023.109985

Zhao G, Zhen JF, Liu XY, Guo JS, Li DD, Xie JP, Xie LX. Protein post-translational modification by lysine succinylation: Biochemistry, biological implications, and therapeutic opportunities. Genes & Diseases. 2023;10:1242-62. https://doi.org/10.1016/j.gendis.2022.03.009

Zhou L, Zhang YF, Yang FH, Mao HQ, Chen Z, Zhang L. Mitochondrial DNA leakage induces odontoblast inflammation via the cGAS-STING pathway. Cell Communication and Signaling. 2021;19. https://doi.org/10.1186/s12964-021-00738-7

Fig. 1 Expression of succinylation in IPF lungs and mitochondrial accumulation in aging AEC of IPF lungs. A HE and Masson observed the pathology of lung tissue in each group. Scale bars: 50 μm. (B) The succinylation modification in IPF lungs was detected by pan-antibody. (C) The expression of SIRT5 in lung tissues of each group was observed by western blotting (n = 6 per group). Quantification is shown in the lower panel. *P < 0.01, IPF group vs. control group. The results are shown as the means ± SD.

Fig. 2 Mitochondrial accumulation in aging AECs of IPF lungs. A Representative immunofluorescence using anti-SP-C (AEC marker; red), anti-PGC-1α (mitochondrial marker; green), anti-P16 (aging marker; green), and anti-SIRT5 (deKsucc marker; green), showing mitochondrial accumulation in aging AEC from IPF lung. The white arrow indicates AEC. Quantification is shown in the right panel. *P < 0.01, IPF group *vs*. control group. Scale bars: 50 μm. **B** Representative TEM (n = 6 per group) in control and IPF AEC (identified by the presence of lamellar bodies). Boxed regions are shown enlarged at the bottom. Scale bars: 500 nm. **C** Frequency of mitochondrial area from AEC in control and IPF lungs (obtained from TEM images). **D** The number of mitochondria per cell (obtained from TEM images) between control and IPF lungs AEC. **E** Percentage of abnormal mitochondria (swollen with evidence of severely disrupted cristae overall mitochondria) (obtained from TEM images). **F** Mitochondrial mass, assessed by mtDNA/gDNA ratio, in isolated AEC from control and IPF lungs. Data represent mean ± SEM (G, H, and I). *P < 0.01, IPF AEC group *vs*. AEC control group.

Fig. 3 SIRT5 and dysfunctional mitochondria change during aging. A Representative HE and Masson trichrome staining from lungs at 7, 12, and 24-month-old mice after BLM infection, showing increased pneumonitis and collagen deposition (blue). Scale bars: 50 μm. **B** Representative immunostaining of lung sections from control and IPF patients using anti-SPC (red; AEC marker) and anti-P16 (green; aging marker) antibodies and anti-PGC-1α (mitochondrial marker; green). The white arrow indicates AEC. Scale bars: 25 μm. **C** Quantitative analysis of immunofluorescence. * $P < 0.05$, 12-month-old mice *vs*. 7-month-old mice. ** $P < 0.01$, 24-month-old mice *vs*. 7-month-old mice.

Fig. 4 Mitochondrial homeostasis is enhanced and SIRT5 expression is downregulated in aging AECs of old mice. A The expression of PGC-1α and TFAM was examined by Western blotting and Quantification of protein levels relative to control. **B** SA-β-gal staining was performed to detect AEC senescence. Scale bars: 25 μm. **C** The AEC from different old mice were stained with MitoTracker deep red. Scale bars: 25 μm. **D** Mitochondrial mass was determined by the rate of MitoTracker deep red fluorescence intensity. Quantification of mitochondrial mass in AEC from different old mice is shown. **E** The AEC from different old mice were stained with mitoSOX probes. Scale bars: 25 μm. **F** Increased mitochondrial mass in old AEC, assessed by mtDNA/gDNA ratio. * $P < 0.05$, AEC of 12-month-old mice *vs*. AEC of 7-month-old mice. ** $P < 0.01$, AEC of 24-month-old mice *vs*. AEC of 7-month-old mice.

Fig. 5 SIRT5-mediated deKsucc protects lung mitochondrial homeostasis in BLM-induced aging model in vivo. A Representative immunofluorescence staining of 12-month-old mice lung sections using anti-SPC (red; AEC marker) and anti-PGC-1α (green; mitochondrial marker), SIRT5 (green; mitochondrial deKsucc marker). The experiment was repeated three times. Bar=50μm. **B** Quantitative analysis of immunofluorescence. ** $P < 0.01$, BLM group *vs*. BLM + LV-*SIRT5*pcDNA group. **C** The different groups of 12-month-old mice were stained with MitoTracker deep red.

The experiment was repeated three times. Bar=50μm. **D** Quantification of mitochondrial mass in different groups of 12-month-old mice is shown in the right panel. $^{**}P < 0.01$, BLM group *vs*. BLM + LV-*SIRT5*pcDNA group.

Fig. 6 SIRT5-mediated deKsucc protects lung mitochondrial homeostasis in BLM induced aging model in vitro A The expression of PGC-1α, TFAM, and SIRT5 in different groups was examined by Western blotting. Quantification is shown in the right panel. **B** Representative immunofluorescence images in different groups by staining of PGC-1α (red), TFAM (green), and SIRT5 (green). Quantitative analysis of immunofluorescence is shown in the right panel. Bar=25μm. **C** Representative fluorescence shows mitochondrial mass and ROS production in different groups. Quantification of mitochondrial mass in AEC is in the right panel. Scale bar=25μm. **D** mitochondrial mass in different groups was studied using TEM. For TEM analyses, boxed regions are shown enlarged at lower and indicate abnormal characteristics of swollen shape and fragmented cristae in mitochondria. Area of AEC mitochondria, percentage of abnormal mitochondria (swollen with evidence of severely disrupted cristae overall mitochondria), and number of mitochondria per cell from TEM images. The experiment was repeated three times. Scale bars=500 nm. **E** Increased mitochondrial mass in different groups, assessed by mtDNA/gDNA ratio. The experiment was repeated three times. $^{*}P < 0.01$, Control group *vs*.BLM group. $^{**}P < 0.01$, BLM group *vs*. BLM + LV-*SIRT5*pcDNA group.

Fig. 7 SIRT5-mediated deKsucc inhibits AEC senescence in vivo and in vitro. A Representative immunofluorescence images on 12-month-old mice lung. AEC were labeled with SP-C (red) and p16 (green). Bar=50μm. Quantification is shown in the lower panel. **B** Pulmonary fibrosis was determined by HE staining and Masson's trichrome staining. Representative images of four independent experiments are shown. Bar=50μm. Quantifcation is shown in the right panel, and quantifcation of pulmonary fibrosis by measuring fibrotic area in lung sections. **C** Representative staining micrographs show AEC senescence of SA-β-gal activity. Scale bar, 25 μm. **D** The

expression of p16 was examined by Western blotting. β-actin was used as the loading control. Quantification of protein levels relative to control. **E** The expression of p16 was examined by representative immunofluorescence images. The experiment was repeated three times. Bar=25 μm. **F** Representative immunofluorescence images on CM-treated AEC by dual staining of Collagen I (red) and α-SMA (green). Quantification is shown in the lower panel. The experiment was repeated three times. Bar = 25 μm. *$P < 0.01$, Control group *vs*.BLM group. **$P < 0.01$, BLM group *vs*. BLM + LV-*SIRT5*pcDNA group.

Fig. 8 Detection of succinylated modified proteins in IPF lung. A Motif analysis of succinylated proteins. **B** Succinylated proteins. **C** The subcellular locations of the succinylated sites proteins. **D** GO enrichment analysis of the succinylated proteins in IPF tissues. **E** Top 20 enriched items for KEGG analysis of succinylated modified proteins

Fig. 9 SIRT5 regulates the expression of HSD17B8 and GRHPR. A Visualization of relative protein abundances measured by PRM mass spectrometry in succinylated samples between control lung tissues and IPF lung tissues. Each group contains three samples. The asterisks indicate the level of significance. *$P < 0.01$, Control group *vs*. IPF group. **$P < 0.01$, Control group *vs*. IPF group. **B** HSD17B8 and GRHPR levels in total cell lysates were assessed using western blot analyses. The succinylation analysis of the immunoprecipitated HSD17B8 and GRHPR proteins. HSD17B8 and GRHPR were immunoprecipitated from whole-cell lysates using anti-HSD17B8 and GRHPR antibodies, respectively. The blots were probed with succinylation. *$P < 0.01$, Control group *vs*. BLM group. **$P > 0.05$, BLM group *vs*. LV-*SIRT5*pcDNA+BLM group (HSD17B8 and GRHPR). #$P < 0.01$, Control group *vs*. BLM group. ##$P < 0.01$, BLM group *vs*. LV-*SIRT5*pcDNA+BLM group (HSD17B8-succinylation and GRHPR-succinylation). All data are presented as the mean ± SEM of three independent experiments. Quantification is shown in the lower panel. Each experiment was performed in triplicate.

S1: SIRT5 expression assessed in vitro and in vivo. A Fluorescently labeled *SIRT5*pcDNA was transfected into AEC. **B** SIRT5 expression assessed using RT-PCR analysis *$P < 0.05$, **$P < 0.01$. **, control group vs. the LV-*SIRT5*pcDNA; *, the BLM group vs. the LV-*SIRT5*pcDNA + BLM group. The results are shown as the means ± SD.

S2: The succinylated proteins identified in this study for the first time.

S3: Supplementary 3. KEGG analysis of the succinylated proteins in IPF tissues.

S4: GO enrichment analysis of the succinylated proteins in IPF tissues.

S5: Quantitative verification results of PRM

Figures

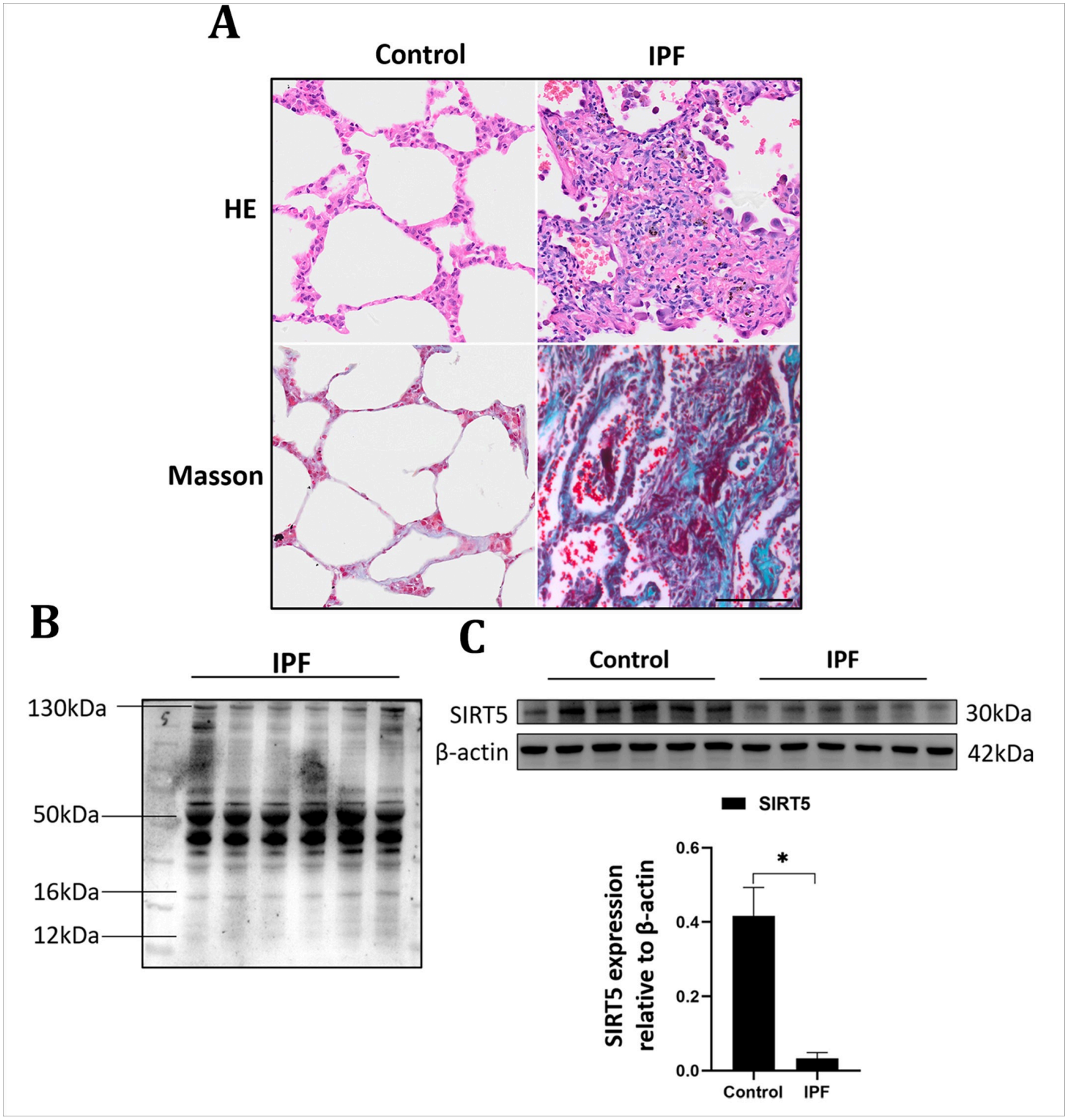


Figure 1

Expression of succinylation in IPF lungs and mitochondrial accumulation in aging AEC of IPF lungs. A HE and Masson observed the pathology of lung tissue in each group. Scale bars: 50 μm. (B) The succinylation modification in IPF lungs was detected by pan-antibody. (C) The expression of SIRT5 in

lung tissues of each group was observed by western blotting (n = 6 per group). Quantification is shown in the lower panel. *P < 0.01, IPF group vs. control group. The results are shown as the means ± SD.

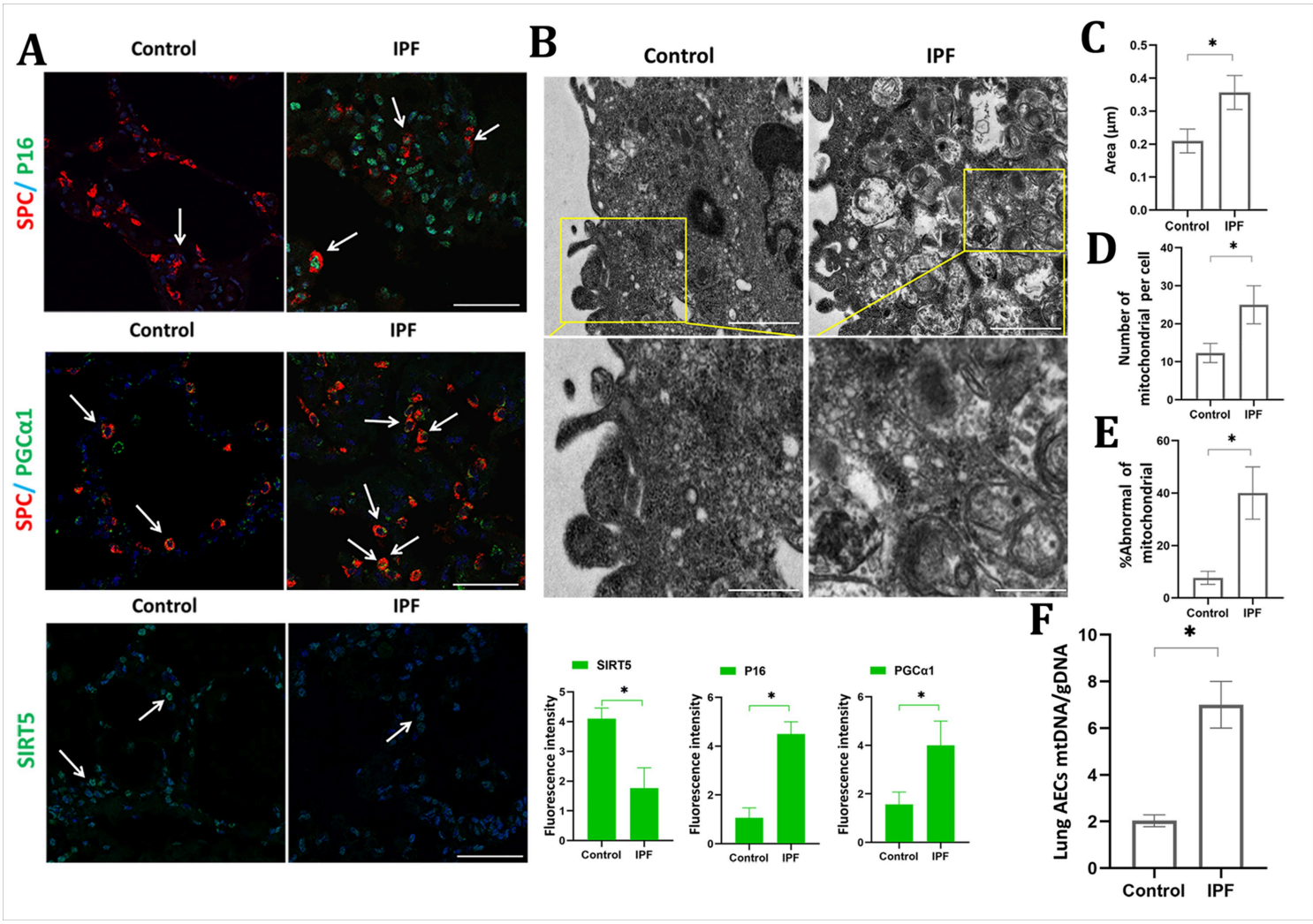


Figure 2

Mitochondrial accumulation in aging AECs of IPF lungs. A Representative immunofluorescence using anti-SP-C (AEC marker; red), anti-PGC-1α (mitochondrial marker; green), anti-P16 (aging marker; green), and anti-SIRT5 (deKsucc marker; green), showing mitochondrial accumulation in aging AEC from IPF lung. The white arrow indicates AEC. Quantification is shown in the right panel. *P < 0.01, IPF group vs. control group. Scale bars: 50 μm. B Representative TEM (n = 6 per group) in control and IPF AEC (identified by the presence of lamellar bodies). Boxed regions are shown enlarged at the bottom. Scale bars: 500 nm. C Frequency of mitochondrial area from AEC in control and IPF lungs (obtained from TEM images). D The number of mitochondria per cell (obtained from TEM images) between control and IPF lungs AEC. E Percentage of abnormal mitochondria (swollen with evidence of severely disrupted cristae overall mitochondria) (obtained from TEM images). F Mitochondrial mass, assessed by mtDNA/gDNA ratio, in isolated AEC from control and IPF lungs. Data represent mean ± SEM (G, H, and I). *P < 0.01, IPF AEC group vs. AEC control group.

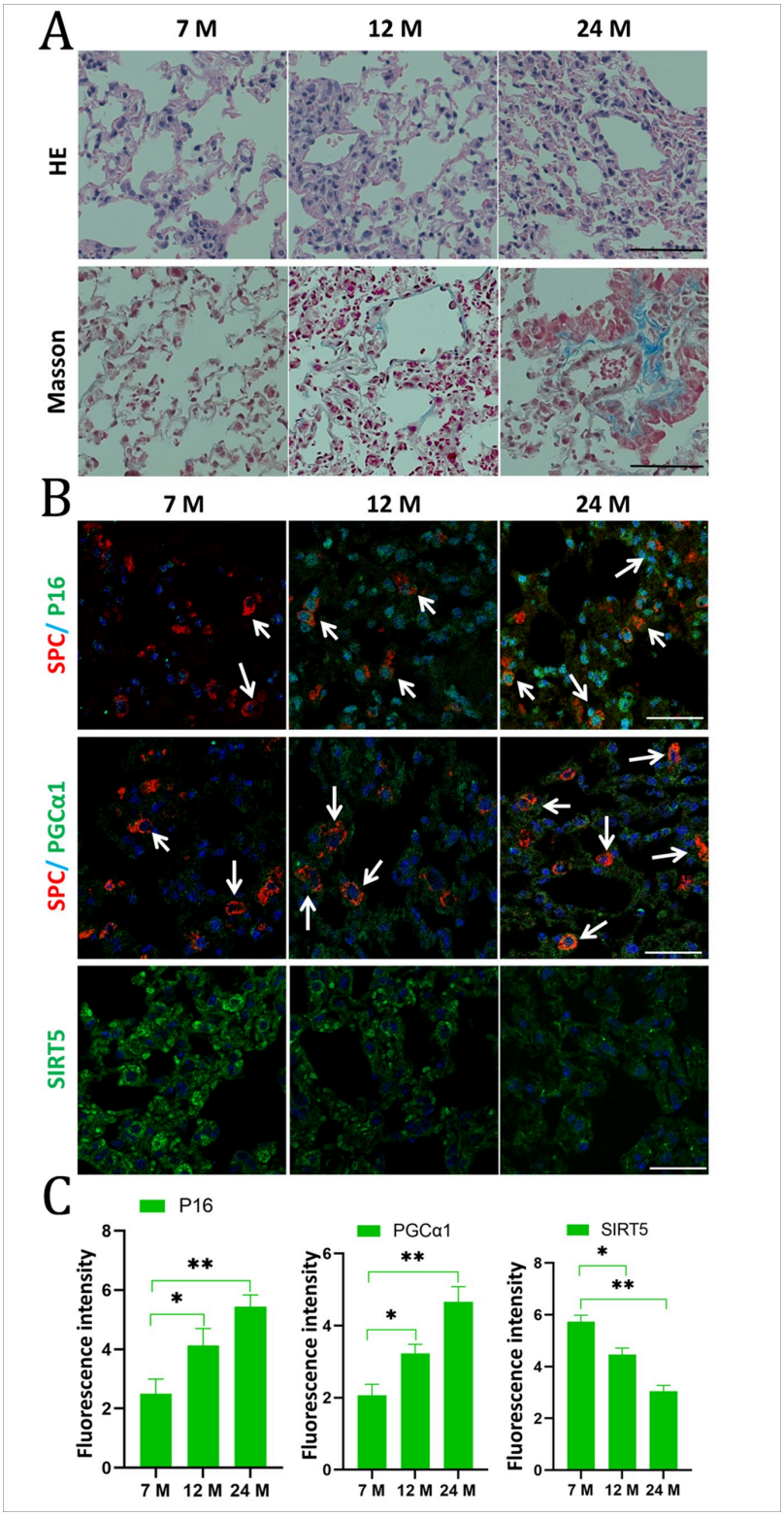


Figure 3

SIRT5 and dysfunctional mitochondria change during aging. A Representative HE and Masson trichrome staining from lungs at 7, 12, and 24-monthold mice after BLM infection, showing increased pneumonitis and collagen deposition (blue). Scale bars: 50 μm. B Representative immunostaining of lung sections from control and IPF patients using anti-SPC (red; AEC marker) and anti-P16 (green; aging marker) antibodies and anti-PGC-1α (mitochondrial marker; green). The white arrow indicates AEC. Scale bars: 25

μm. C Quantitative analysis of immunofluorescence. * P < 0.05, 12-month-old mice vs. 7-month-old mice. **P < 0.01, 24-month-old mice vs. 7-month-old mice.

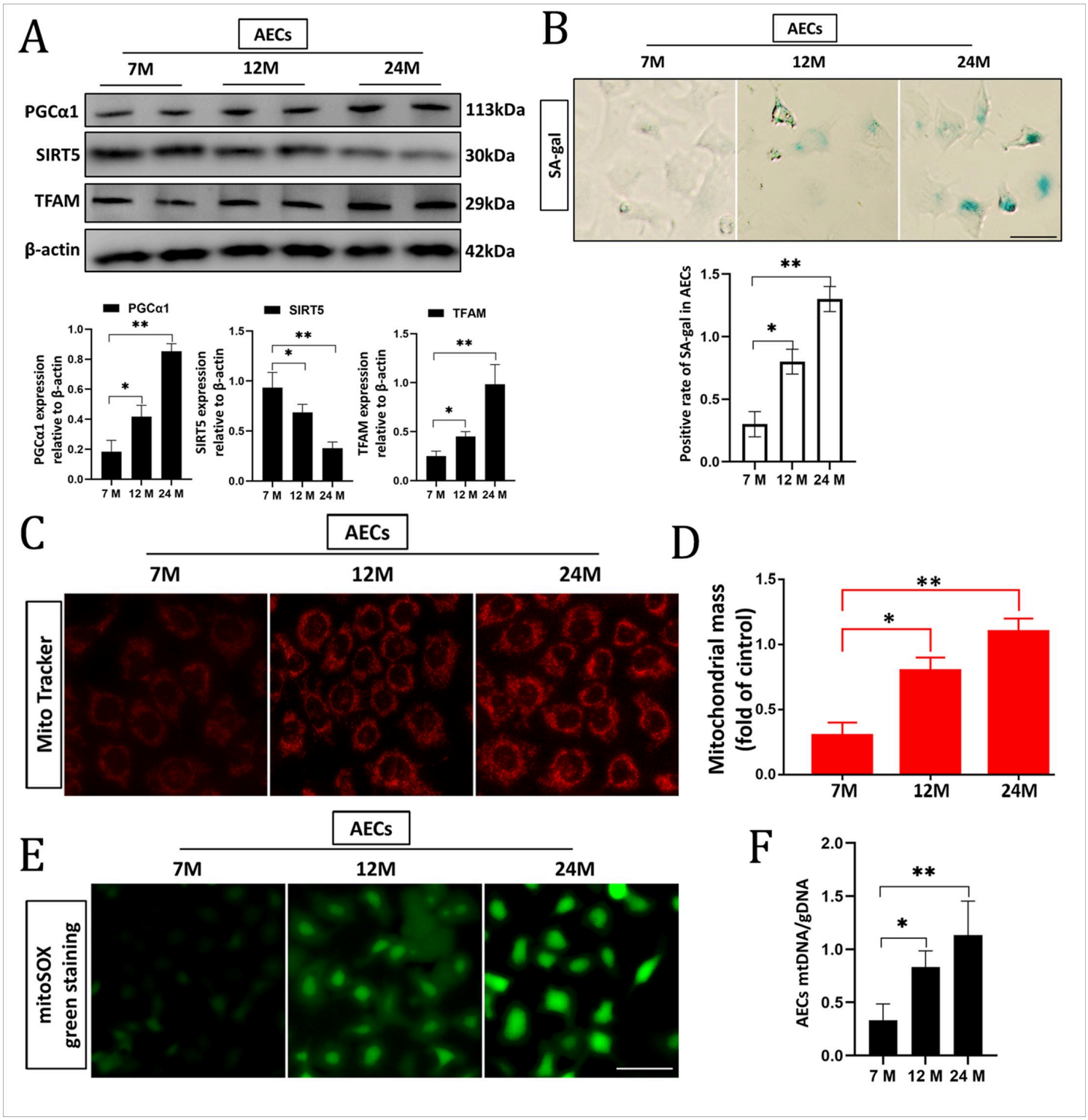


Figure 4

Mitochondrial homeostasis is enhanced and SIRT5 expression is downregulated in aging AECs of old mice. A The expression of PGC-1α and TFAM was examined by Western blotting and Quantification of protein levels relative to control. B SA-β-gal staining was performed to detect AEC senescence. Scale

bars: 25 μm. C The AEC from different old mice were stained with MitoTracker deep red. Scale bars: 25 μm. D Mitochondrial mass was determined by the rate of MitoTracker deep red fluorescence intensity. Quantification of mitochondrial mass in AEC from different old mice is shown. E The AEC from different old mice were stained with mitoSOX probes. Scale bars: 25 μm. F Increased mitochondrial mass in old AEC, assessed by mtDNA/gDNA ratio. *P < 0.05, AEC of 12-month-old mice vs. AEC of 7-month-old mice. **P < 0.01, AEC of 24-month-old mice vs. AEC of 7-month-old mice.

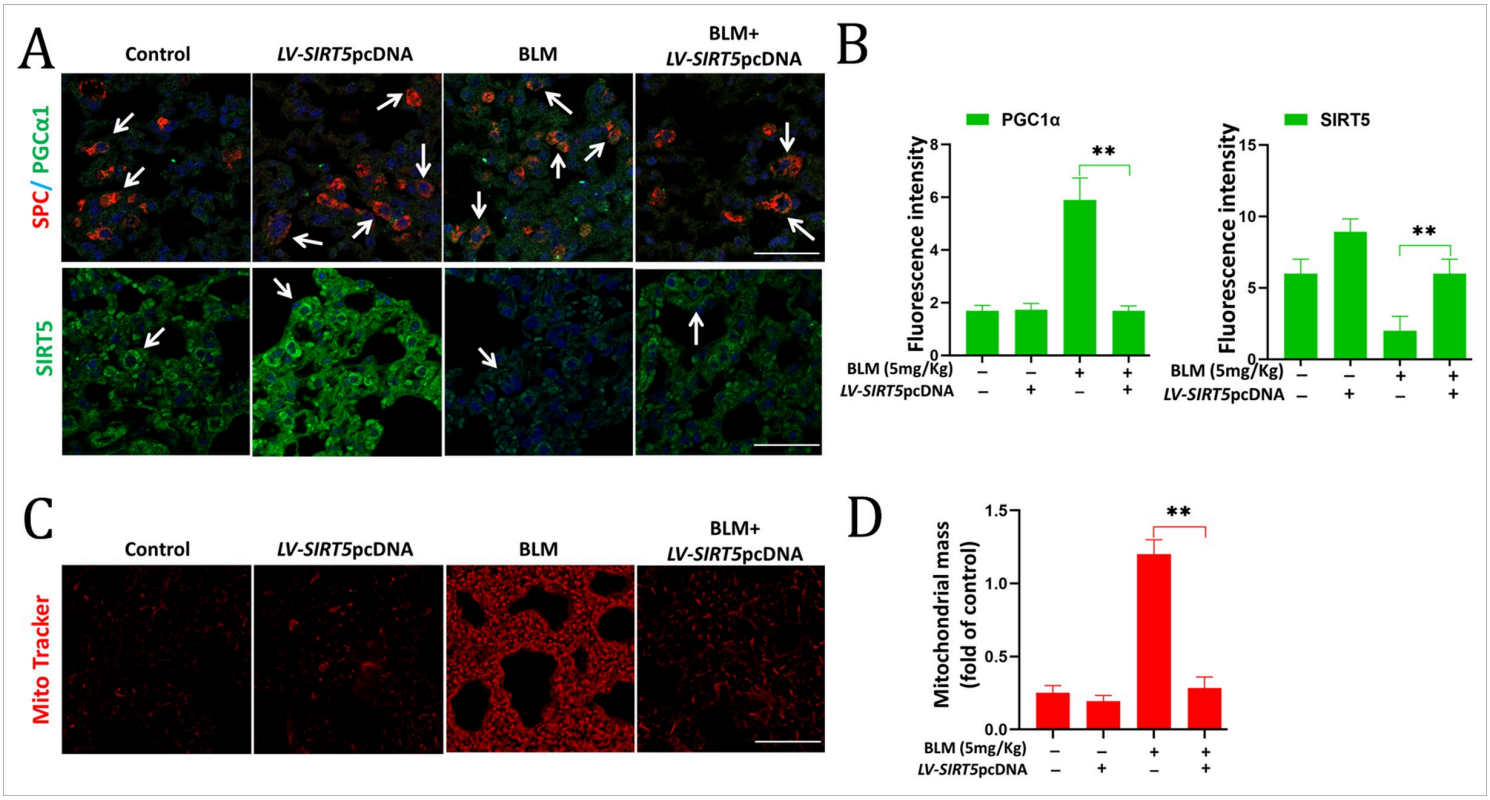


Figure 5

SIRT5-mediated deKsucc protects lung mitochondrial homeostasis in BLMinduced aging model in vivo. A Representative immunofluorescence staining of 12- month-old mice lung sections using anti-SPC (red; AEC marker) and anti-PGC-1α (green; mitochondrial marker), SIRT5 (green; mitochondrial deKsucc marker). The experiment was repeated three times. Bar=50μm. B Quantitative analysis of immunofluorescence. **P < 0.01, BLM group vs. BLM + LV-SIRT5pcDNA group. C The different groups of 12-month-old mice were stained with MitoTracker deep red. The experiment was repeated three times. Bar=50μm. D Quantification of mitochondrial mass in different groups of 12-month-old mice is shown in the right panel. **P < 0.01, BLM group vs. BLM + LV-SIRT5pcDNA group.

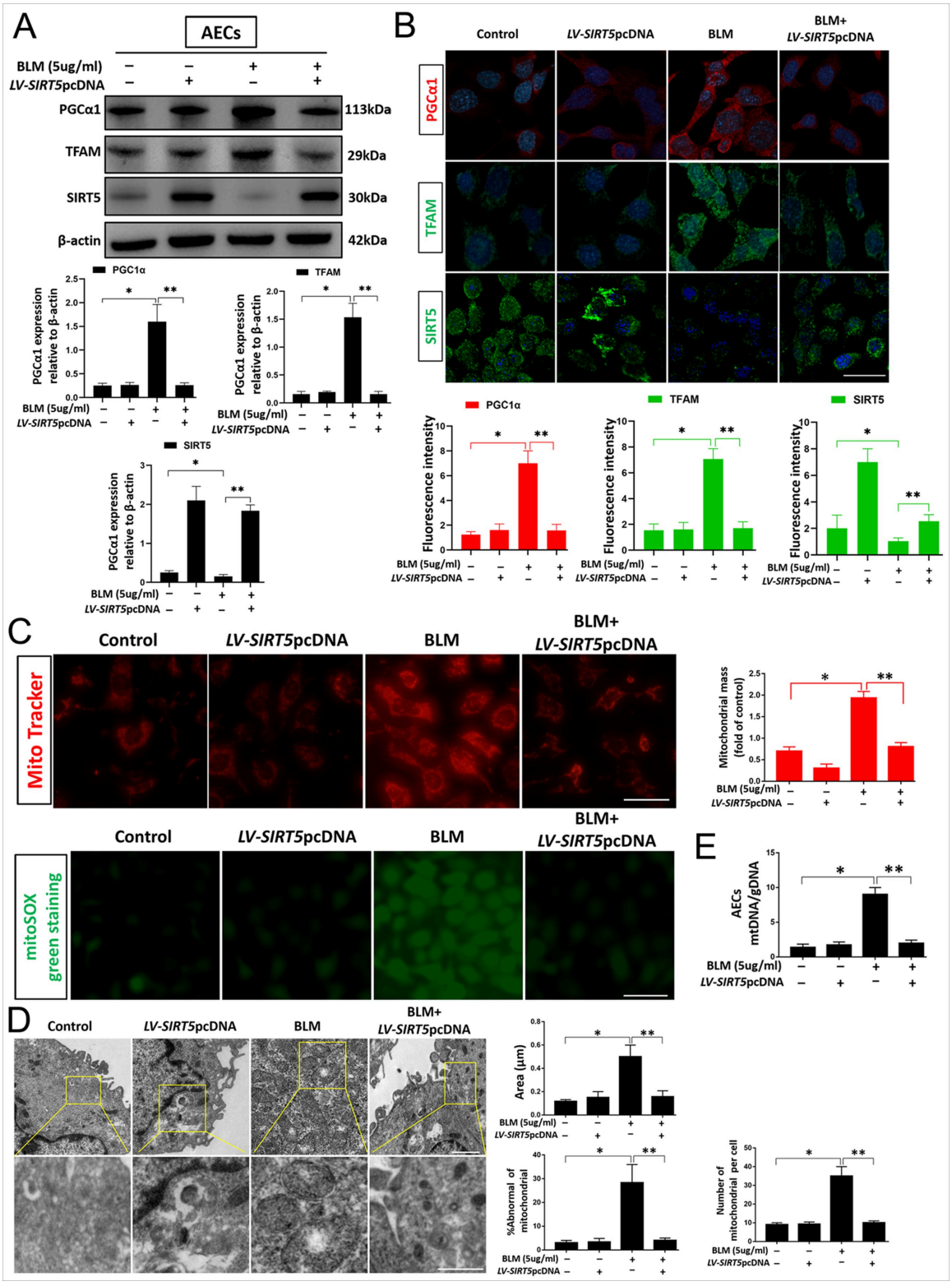


Figure 6

SIRT5-mediated deKsucc protects lung mitochondrial homeostasis in BLM induced aging model in vitro A The expression of PGC-1α, TFAM, and SIRT5 in different groups was examined by Western blotting. Quantification is shown in the right panel. B Representative immunofluorescence images in different groups by staining of PGC-1α (red), TFAM (green), and SIRT5 (green). Quantitative analysis of immunofluorescence is shown in the right panel. Bar=25μm. C Representative fluorescence shows

mitochondrial mass and ROS production in different groups. Quantification of mitochondrial mass in AEC is in the right panel. Scale bar=25μm. D mitochondrial mass in different groups was studied using TEM. For TEM analyses, boxed regions are shown enlarged at lower and indicate abnormal characteristics of swollen shape and fragmented cristae in mitochondria. Area of AEC mitochondria, percentage of abnormal mitochondria (swollen with evidence of severely disrupted cristae overall mitochondria), and number of mitochondria per cell from TEM images. The experiment was repeated three times. Scale bars=500 nm. E Increased mitochondrial mass in different groups, assessed by mtDNA/gDNA ratio. The experiment was repeated three times. *P < 0.01, Control group vs.BLM group. **P < 0.01, BLM group vs. BLM + LV-SIRT5pcDNA group.

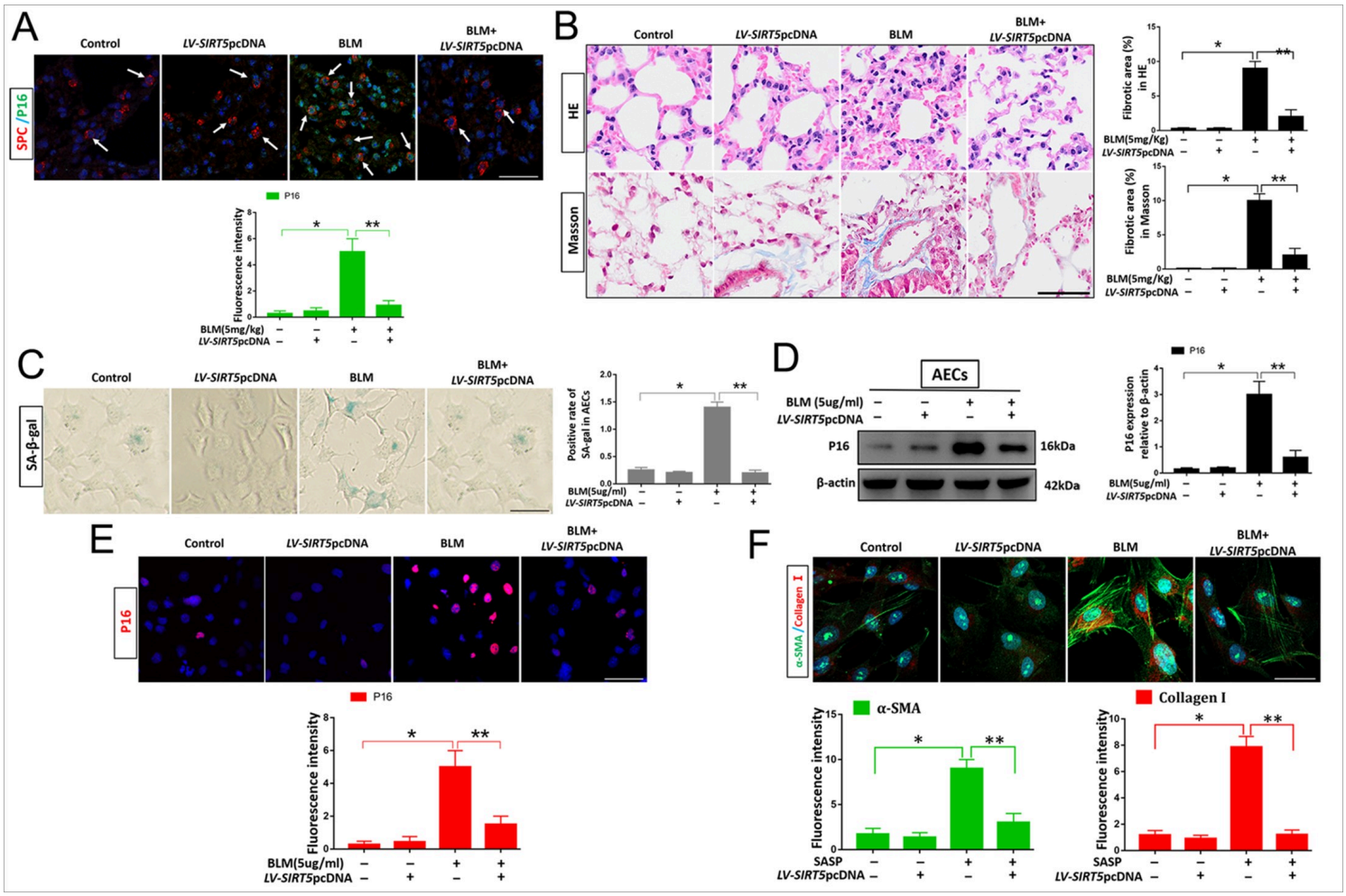


Figure 7

SIRT5-mediated deKsucc inhibits AEC senescence in vivo and in vitro. A Representative immunofluorescence images on 12-month-old mice lung. AEC were labeled with SP-C (red) and p16 (green). Bar=50μm. Quantification is shown in the lower panel. B Pulmonary fibrosis was determined by HE staining and Masson's trichrome staining. Representative images of four independent experiments are shown. Bar=50μm. Quantifcation is shown in the right panel, and quantifcation of pulmonary fibrosis by measuring fibrotic area in lung sections. C Representative staining micrographs show AEC senescence of SA-β-gal activity. Scale bar, 25 μm. D The expression of p16 was examined by Western blotting. β-actin was used as the loading control. Quantification of protein levels relative to control. E The

expression of p16 was examined by representative immunofluorescence images. The experiment was repeated three times. Bar=25 μm. F Representative immunofluorescence images on CM-treated AEC by dual staining of Collagen I (red) and α-SMA (green). Quantification is shown in the lower panel. The experiment was repeated three times. Bar = 25 μm. *P < 0.01, Control group vs.BLM group. **P < 0.01, BLM group vs. BLM + LV-SIRT5pcDNA group

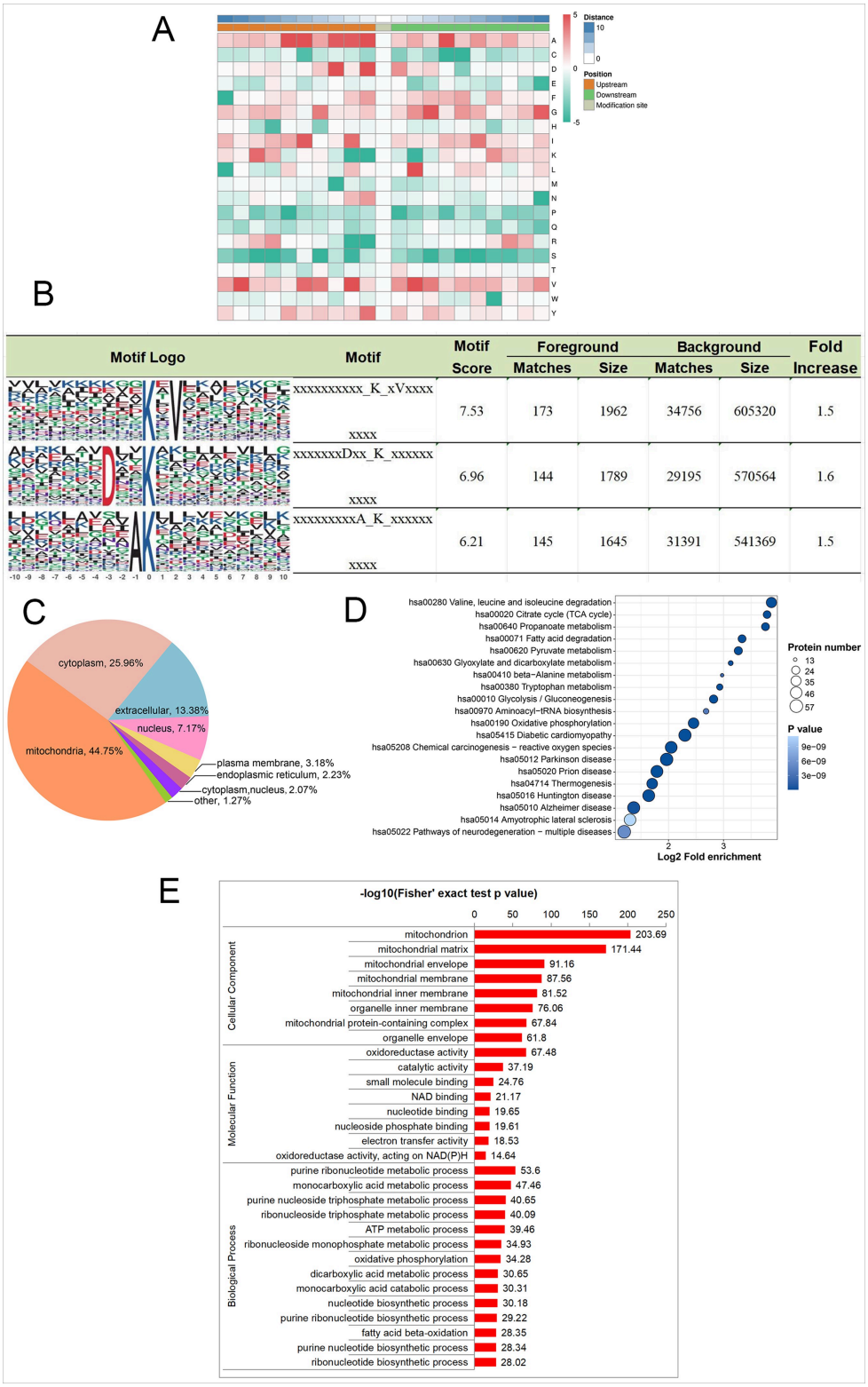


Figure 8

Detection of succinylated modified proteins in IPF lung. A Motif analysis of succinylated proteins. B Succinylated proteins. C The subcellular locations of the succinylated sites proteins. D GO enrichment analysis of the succinylated proteins in IPF tissues. E Top 20 enriched items for KEGG analysis of succinylated modified proteins

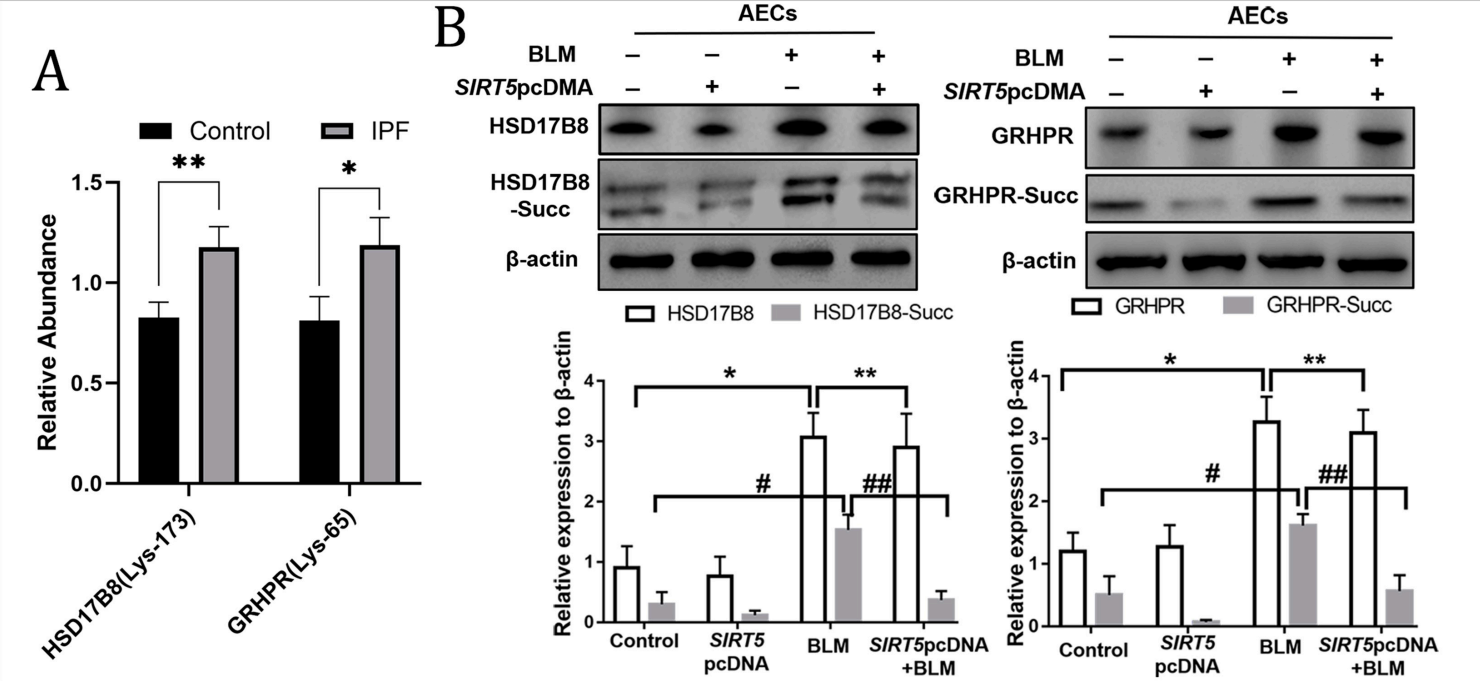


Figure 9

SIRT5 regulates the expression of HSD17B8 and GRHPR. A Visualization of relative protein abundances measured by PRM mass spectrometry in succinylated samples between control lung tissues and IPF lung tissues. Each group contains three samples. The asterisks indicate the level of significance. *P < 0.01, Control group vs. IPF group. **P < 0.01, Control group vs. IPF group. B HSD17B8 and GRHPR levels in total cell lysates were assessed using western blot analyses. The succinylation analysis of the immunoprecipitated HSD17B8 and GRHPR proteins. HSD17B8 and GRHPR were immunoprecipitated from whole-cell lysates using anti-HSD17B8 and GRHPR antibodies, respectively. The blots were probed with succinylation. *P < 0.01, Control group vs. BLM group. **P0.05, BLM group vs. LV-SIRT5pcDNA+BLM group (HSD17B8 and GRHPR). #P < 0.01, Control group vs. BLM group. ##P < 0.01, BLM group vs. LV-SIRT5pcDNA+BLM group (HSD17B8-succinylation and GRHPRsuccinylation). All data are presented as the mean ± SEM of three independent experiments. Quantification is shown in the lower panel. Each experiment was performed in triplicate.

Supplementary Files

This is a list of supplementary files associated with this preprint. Click to download.

- S11.jpg